Rodríguez-Sánchez, M. R., Sánchez-González, A., González-Gómez, P. A., Marugán-Cruz, C. & Santana, D. (2017). Thermodynamic and economic assessment of a new generation of subcritical and supercritical solar power towers. *Energy*, 118, pp. 534–544.

DOI: 10.1016/j.energy.2016.10.079

Thermodynamic and economic assessment of a new generation of subcritical and supercritical solar power towers

M.R. Rodríguez-Sánchez, A. Sánchez-González, P.A. González-Gómez, C. Marugán-Cruz, D. Santana

Energy Systems Engineering Group (ISE), Department of Fluids and Thermal Engineering, Universidad Carlos III of Madrid. Av. Universidad 30, Leganés, 28911 Madrid (Spain). Phone number: +34 916246034, Fax: +34916249430, e-mail: mrrsanch@ing.uc3m.es

Abstract

The feasibility of using more efficient Rankine power blocks in solar power towers (SPTs) with molten salt as the heat transfer fluid has been studied as a method for increasing the global efficiency of these power plants. The temperature and pressure of the main steam and the reheating pressure affect the temperature of the molten salt in the receiver; for temperature increase decreasing the receiver efficiency and increasing the power block efficiency. Therefore, a detailed study of these SPTs has been conducted to determine whether the proposed changes increase the global efficiency of the SPTs.

A total of eight different subcritical and supercritical SPTs have been investigated. To set the most important cost of the SPT, the same heliostat field has been used. The receiver geometry has been optimised for each SPT to maximise the heliostat-receiver efficiency, fulfilling the material limitations.

It has been observed that the pressure at the inlet of the turbine increases

the SPT efficiency even more than the temperature. However, special attention has to be paid to the reheating pressure, which is the most influential factor on the SPT efficiency. A high reheating pressure considerably decreases the SPT efficiency. Therefore, the best efficiencies have been obtained for the supercritical SPTs with a low reheating pressure and high temperature. It is closely followed by subcritical SPTs at high pressure and temperature.

The investment cost of the different SPTs also increases with the pressure and the temperature of the PB, with subcritical SPTs being less expensive than supercritical SPTs. However, the cost increase is balanced by the increase in the efficiency. The same cost per kW_e is found in subcritical SPTs working at 16 MPa and in supercritical SPTs with low reheating pressure.

Keywords:
Solar Power Tower; Solar Receiver; Heliostat-Receiver Model; Supercritical Power Block; Molten Salt.

---

1. Introduction

One of the main challenges of solar power towers (SPTs) is reducing the levelized cost of electricity (LCOE) to improve their competitiveness with conventional electricity generation. This can be achieved by increasing the overall efficiency of the SPTs (Short and Packey, 1995). The efficiency of a SPT can be approximately defined as the product of the efficiencies of the three main subsystems of the plant, namely, heliostat field, receiver, and power block (PB), as shown in Equation 1. Optimization on terms of efficiency has to be focused on improving at least one of these subsystems without negatively impacting on the others. A schematic of the main sub-

systems of a SPT can be seen in Figure 1.

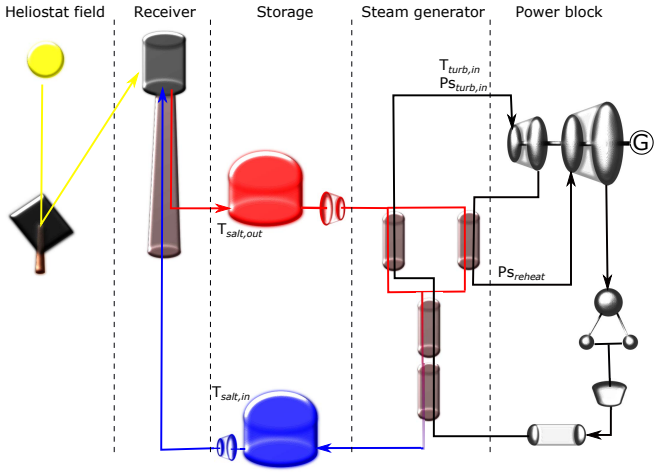

Figure 1: Schematic of the main subsystems of a solar power tower plant.

$$\eta_{SPT} = \eta_{field} \cdot \eta_{rec} \cdot \eta_{PB} \tag{1}$$

Over the past decades, numerous proposals to increase the efficiency of the different subsystems of SPTs have been investigated. For example, Sánchez and Romero (2006) developed a methodology to create heliostat layouts based on the yearly energy available, and Boerema et al. (2013) and Rodríguez-Sánchez et al. (2014c) investigated new receiver designs using different tube diameters and bayonet tubes, respectively. Neises et al. (2014) tested new materials for the receivers, Boerema et al. (2012) compared different heat transfer fluids (HTFs), and McGovern and Smith (2012) studied the effects of increasing the outlet temperature of the HTF to employ a supercritical steam PB.

Modern turbines can work at high pressure and temperature, thus increas-

ing the efficiency of the PB with respect to traditional subcritical turbines. It should be taken into account that the advantage of supercritical steam can vanish for mid-scale power plants, around 20-25 MW_e. For small flow rate and low specific volume of steam, as in the case of mid-size turbines and supercritical water pressure respectively, the flow coefficient is low and hence lead to low turbine efficiency (Bloch and Singh, 2009). Despite this, it is feasible to adapt existing mid-turbines for supercritical steam in mid-size solar power plants (Pacheco et al., 2013). Singer et al. (2014) noted that these turbines could be integrated in power plants with central receiver technology; he studied external and cavity receivers working at 565 °C, 600 °C and 620 °C in several 125 MW_e SPTs, obtaining improvements of approximately 2% in the global plant efficiency; however, they did not obtain a reduction in the LCOE. Neises et al. (2014) analysed the driving factors of a SPT, whose HTF was CO_2 at 25 MPa and 650 °C, to investigate the viability of these SPTs. Kolb (2011) examined the implementation of a modern PB in a hypothetical 1,000 MW_{thl} SPT that would use molten salt as the HTF; he found improvements of 5.4% in the efficiency of the advanced SPTs, although the optical efficiency of the field decreased with the size. Pacheco et al. (2013) analysed 14 different subcritical and supercritical 250 MW_e molten-salt SPTs; they examined the effects of modifying the pressure and temperature of the steam, the final feed-water and the return temperature of the salt. Pacheco et al. (2013) found that supercritical SPTs have better efficiencies and lower LCOEs than subcritical SPTs. These results were supported by Peterseim and Veeraragavan (2015) for 250 MW_e SPTs. Therefore, there appears to be a disparity of results in the application of a supercritical PB in SPTs.

In this study, the feasibility of increasing the global SPT efficiency by improving the PB efficiency has been analysed. A Crescent Dunes-like 110 MW_e subcritical SPT has been compared with other seven subcritical and supercritical SPTs, which possess the same heliostat field size. The analysed SPTs are the combination of different steam pressures (12, 16 and 24 MPa) and temperatures (548 and 580 °C). Moreover, in the supercritical PB, two different reheating pressures (7 and 4.5 MPa) have been tested.

The optimum receiver design has been selected for each studied case, following the design guidelines proposed by Rodríguez-Sánchez et al. (2014a). Furthermore, in agreement with the operational conditions of the receiver, different receiver feed pump systems have been selected for each of the analysed SPTs (Rodríguez-Sánchez et al., 2014d).

The heliostat-receiver efficiency using an advanced PB has been studied not only for the design point (nominal load) but also for the entire range of operational conditions covered by the receiver. Finally, the investment cost of each SPT has been calculated to evaluate the viability of the different configurations analysed.

2. Description of the SPTs studied

In this work, different molten-salt SPTs have been analysed to find the SPT design that maximises the global efficiency of the plant and minimises its investment cost. The reference SPT is a 110 MW_e subcritical plant with a solar multiple of 3.8 based on Crescent Dunes (NREL, 2011), located in Tonopah at 38.24° N latitude and 117.35° W longitude. The steam turbine operates with a rated output of 125 MW and a speed of 3600 r.p.m. The

inlet temperature and pressure of the turbine are 540 °C and 11.6 MPa, respectively. Moreover, it has three bleeding at pressures of 3.9 MPa (HP turbine), 0.15 MPa (LP turbine) and 0.04 MPa (LP turbine) and a final exhaust condensing pressure of 0.013 MPa; where the pressure of the first bleeding corresponds to the reheating pressure.

The reference SPT (Sub1) has been compared with seven other SPTs. In these plants, the temperature and/or the pressure of the steam at the inlet of the turbine and in the reheat have been modified, as shown in Table 1.

The design point selected for all the SPTs is the spring equinox at solar noon (Winter et al., 1991). The same heliostat field has been used for all the SPTs analysed. Therefore, depending on the temperature and pressure ranges of each SPT, the net power has different values. The heliostat field consists of is 10,301 rectangular mirrors, 11.28 m width and 10.36 m height, surrounding the tower. Crescent Dunes' field layout has been gathered from scaled aerial images. Each heliostat is gathered by 35 flat facets, which gives the curvature needed to reduce the spillage losses.

Note that the inlet and exit conditions of the molten salt in receivers Sub3 and Sup3 and in receivers Sub4 and Sup4 are the same. Consequently, there are only 6 different receivers, and the difference in these SPTs is the PB. The different steam conditions correspond to the typical operating ranges of existing turbines (Retzlaff and Ruegger, 1996; Alexe and Cenusa, 2008). Variations in the steam pressure and temperature also affect the HTF temperature on the receiver, as shown in Table 1.

The cylindrical external receivers are formed by vertical tubes arranged in panels. The base of all the analysed receivers is situated on a tower that is 180

Table 1: Main parameters of the eight subcritical and supercritical SPTs analysed.The reheating pressure has been selected according to Alexe and Cenusa (2008); Retzlaff and Ruegger (1996), and the PB block efficiency has been obtained from Sano (2009); Pacheco et al. (2013)

	Sub1	**Sub2**	**Sub3**	**Sub4**	**Sup1**	**Sup2**	**Sup3**	**Sup4**
$\mathbf{T}_{salt,in}$ [°C]	290	290	307	307	405	405	307	307
$\mathbf{T}_{salt,out}$ [°C]	565	600	565	600	565	600	565	600
$\mathbf{T}_{turb,in}$ [°C]	548	580	548	580	548	580	548	580
$\mathbf{Ps}_{turb,in}$ [MPa]	12	12	16	16	24	24	24	24
$\mathbf{Ps}_{reheat}$ [MPa]	3.5	4.66	3.5	4.66	7	7	4.5	4.5
η_{PB} [%]	39.4	40.1	42.2	42.9	44.6	45.2	43.8	44.6

m high. All the studied receivers employ solar salt (60% $NaNO_3$ - 40% KNO_3) as the HTF, whose properties has been calculated using the equations pointed by Zavoico (2001). Olivares (2012) reported that solar salt in atmospheric air and temperatures lower than 650 °C has a constant nitrite-nitrate ratio, and above that temperature, there is an important decomposition of the salt. However, none of the investigated SPTs exceeded the maximum allowable temperature of 650 °C.

All the receivers are 20.5 m high, with an aspect ratio of 1.14, which is within the recommended range (Lovegrove and Stein, 2012). The remainder of the parameters that determine the receiver geometry (material, number of panels, number of tubes, tube diameter and tube thickness) have been selected to maximise the combined heliostat-receiver efficiency for each PB and to minimise the parasitic consumption of the feed pump system.

Table 2 summarises the different parameters for optimising the receivers.

The flow pattern of the analysed receivers consists of two north-to-south flow paths without crossovers (Rodríguez-Sánchez et al., 2015b); thus, the number of panels must be even. Moreover, to optimise the receiver geometry, 8 nominal diameters ranging from 8.89 to 2.13 cm and 7 different nominal thickness from 1.24 to 9.09 mm have been tested.

Table 2: Geometry parameters studied to optimise the receiver design.

Material	**Number of panels** (N_p)	**Tube diameter** [**mm**] (d_{ext})	**Tube thickness** [**mm**] (th)
Inconel 625	14	88.9	1.24
Alloy 800H	16	73	1.65
Haynes 230	18	60.3	2.11
	20	48.3	2.77
	22	42.2	3.73
	24	33.4	4.78
		26.7	9.09
		21.3	

Once the optimum receiver of each SPT is defined, the nominal mass flow rate and the configuration of the feed pump system of each receiver are obtained, as well as the steam mass flow rate and the nominal size of each PB.

The receiver feed pump system of subcritical SPTs is generally formed by several centrifugal high-pressure vertical pumps operating in parallel. In

the case of Crescent Dunes (reference SPT), the pumping system consists of four pumps working in parallel. One of these pumps is only used in the case of a breakdown of one of the other three pumps; therefore, it has not been taken into account in this study. The GVSO vertical pump from the company Friatec has been used for this study (Aliaxis, 2016). The nominal conditions of this pump are a head of 330 m, a volume flow rate of 820 m^3/h and a maximum efficiency of 75.3%. The characteristic curves of this pump are presented in Figure 2. For the different SPTs analysed, the same single pump has been used. However, the pumping system configuration has been modified, adding new pumps in parallel (pr) for larger mass flow rates and new pumps in series (sr) for higher pressure drops.

A subcritical PB generally consists of a single reheat with 5 closed and 1 open feed water heaters, whereas a supercritical PB consists of a single reheat with 7 closed and 1 open feed water heaters (Kolb, 2011). Different subcritical steam generator designs for SPTs are available in the literature. A technical report published by Sandia National Laboratories presents various steam generator designs, performed by different suppliers for 100 MW_e commercial plant (Bechtel corporation, 1993). For example, ABB Lummus proposed a U-tube kettle boiler and U-tube/straight shell heat exchangers for the preheater, superheater and reheater. The main advantage of this design is the lowest investment cost when compared with the other designs. The main disadvantage is the high thermal stress produced in the single tube-sheet.

However, only one supercritical steam generator design has been found in the literature. The design is based on once-through-technology steam

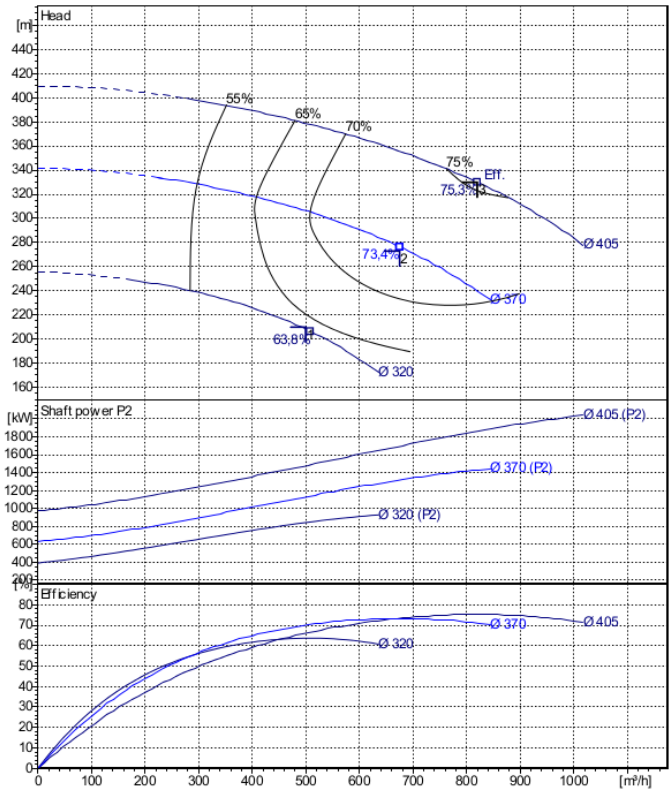

Figure 2: Characteristic curves of a GVSO vertical pump: head, power and efficiency as a function of the volumetric flow rate and the r.p.m of the pump (Friatec, personal communication).

generator using molten salt as heating fluid and was developed by Siemens (Pacheco et al., 2013). This design integrates the preheater, the evaporator and the superheater in a single pressure vessel. The molten salt flows on shell side with tubes in a cross-counter-flow configuration. The reheater is arranged in parallel with the steam generation line.

3. SPT model

The receiver and heliostat field work coupled, and thus, both subsystems have to be studied together to increase the global efficiency of the SPT to the greatest extent possible (Rodríguez-Sánchez et al., 2015a). In this study, the combined heliostat field-receiver model developed in Sánchez-González and Santana (2015) and Rodríguez-Sánchez et al. (2014a) has been used. This model allows for controlling the solar flux distribution on the receiver, calculating the wall and salt temperature distribution on the receiver and obtaining the field and receiver efficiencies.

The optical efficiency of the heliostat field is a function of the angle of incidence (cosine factor), the atmospheric attenuation, the spillage losses and the position of neighbour heliostats in the field (shading and blocking factor), as shown in Equations 2 and 3. Sánchez-González and Santana (2015) reported that for a fixed day and hour, the optical losses depend on the number of panels of the receiver and the aiming strategy employed.

$$\eta_h = \rho \cdot cos(\beta) \cdot \eta_{at} \cdot \eta_{s\&b} \cdot \eta_{sp} \tag{2}$$

$$\eta_{field} = \frac{\sum_{h=1}^{N_h} \eta_h}{N_h} \tag{3}$$

The flux density distribution on the receiver has been modelled as a circular Gaussian distribution convolved into the effective error. A symmetric aiming strategy about equator of the cylindrical receiver has been obtained by pointing heliostats in such a way that the beam circumference was tangential to the upper (odd rows) or the lower (even rows) receiver edges. Beam radius has been estimated on k aiming factor, parameter ranging between

0 and 3 (Sánchez-González and Santana, 2015), where k=3 is equivalent to single equatorial aiming and k=0 involves double aiming to upper and lower receiver edges. The equatorial aiming (k=3) reduces the spillage losses but may cause receiver overheating; therefore, the aiming points should be scattered. As the aiming factor is reduced (multi-aiming strategy), the spillage losses increase, but receiver damages are less likely. Aiming factors from 3 to 1 in half point increments have been tested in the investigated receivers, which modifies the spillage efficiency from 99.7% to 84.13%. Figure 3 shows the solar flux intercepted by a receiver of 18 panels for different aiming strategies. The y axis represents the height of the receiver, the x axis corresponds to the receiver perimeter from north to south ($x = 0$: North), and the colour bar indicates the incident flux density. It can be observed that for low k, the maximum flux decreases and the solar flux becomes more homogeneous.

The behaviour of the different receiver configurations has been analysed using a 2-D simplified thermal model that includes circumferential variations on the tube wall temperature. This model analyses one tube per panel, taking into account the effect of the adjacent tubes (Rodríguez-Sánchez et al., 2014a). Thus, the smallest cell of calculation was formed by two opposite half tubes, the refractory wall and the ambient. The solar flux intercepted by each half tube was the average flux on the panel, i.e. identical operation/performance is assumed for all the tubes within a panel.

The calculation process was iterative. It required as inlet data a first approximation of the wall temperature, the incident flux, and the inlet temperature of the salt. To solve the radiative heat transfer on each panel the net radiation method (Modest, 2003) was used. The wall, film and salt tem-

peratures in the receiver were obtained by the 2D heat transfer problem. The receiver efficiency is determined as the heat absorbed by the HTF from the incident solar flux reflected by the heliostats on the receiver, as shown in Equation 4.

$$\eta_{rec} = \frac{P_{abs}}{A\phi_{inc}} \tag{4}$$

Once the receiver has been thermally and mechanically designed, the power consumption of the feed pump system can be determined (Equation 5).

$$P_{pump,} = \frac{\dot{Q} H_{pump}}{\eta_{pump}} \tag{5}$$

where $\dot{Q}$ is the volumetric flow rate in the receiver; H_{pump} is the head of the pump, calculated as the sum of the hydrostatic pressure plus the pressure drop in the receiver (Rodríguez-Sánchez et al., 2014d); and η_{pump} is the efficiency of the pump, determined using the curves shown in Figure 2.

Regarding to the PB variations, changes in the temperature or pressure modify the required energy in all the heat exchangers of the steam generators. Thus, the needed heat transfer area varies too. A numeric model has been developed to calculate the heat transfer area to supply the required energy from the steam/water side. Whereas, the representative heat transfer coefficients were selected from Kolb (2011), as well as, the constrains necessary to complete the energy equations for subcritical and supercritical cycles.

The feed water temperature (T_{fw}) is assumed to be 240 °C for turbines working at 548 °C and 300 °C for turbines operating at 580 °C. Moreover, in the evaporator, a pinch point of 7 °C has been selected for the subcritical PB (Kolb, 2011), whereas for the supercritical PB, the temperature difference

between the exit of the molten salt and the inlet of the water steam is 10 °C (Zhang et al., 2013).

The steam generator has been dimensioned to achieve the live and reheat conditions at the inlet of the steam turbine. The output power has been determined using the total thermal energy transferred through the steam generator and the efficiency of the PB. The latter has been selected from Sano (2009) when the inlet of the turbine is 548 °C (Sub1, Sub3 and Sup1), while for the remainder of the SPTs, it has been obtained using the data obtained by Pacheco et al. (2013), as shown in Table 1.

Figure 4 shows the flowchart followed to optimize the global SPT design, it is valid for both subcritcal and supercritical SPTs:

4. Operational limits of the receiver

An optimal receiver design must maximise the heliostat-receiver efficiency, reach the expected outlet temperature of the salt and fulfil the different limits of operation. For an external receiver, the main operational limits are as follows: Reynolds number higher than 10,000 to ensure a turbulent flow regime (Petukhov, 1970), mechanical stress lower than 33% of the material ultimate tensile strength (UTS) (ASME, 2011), film temperature below the limit that increases the rate of the tube corrosion, tube thickness that withstands the maximum pressure of the tubes plus the expected corrosion layer during the service period (Kolb, 2011) and a pressure drop that does not drastically increase the parasitic power consumption of the molten salt pumps.

The mechanical stress is defined as the sum of the different components of the thermal stresses and the pressure stresses (Neises et al., 2014).

The film temperature is the maximum temperature of the salt in the cross section. It occurs in a thin layer close to the tube walls and is responsible for the tube corrosion. The limiting film temperature and the expected corrosion rate have been obtained from the literature: 16.8 μm/year for Inconel 625 at 600 °C (McConohy and Kruizenga, 2014), 20 μm/year for Alloy 800H at 630 °C (Bradshaw, 1987) and 23.6 μm/year for Haynes 230 at 680 °C (McConohy and Kruizenga, 2014).

The minimum allowable tube thickness, th_{min}, is defined as the sum of the minimum thickness allowed by the internal pressure in the tubes, th_{ps}, and the corrosion rate during the entire operational life, th_{corr}; see Equations 6 and 7 (Kolb, 2011),

$$th_{min} = th_{ps} + th_{corr} \tag{6}$$

$$th_{ps} \geq \frac{Ps_{max} d_{ext}}{2S_{max}} \tag{7}$$

where S_{max} corresponds to the maximum allowable stress of the tube material (ASME, 2011) and Ps_{max} represents the maximum pressure in the receiver.

5. Results

In this section, the optimal receiver design for each of the eight SPTs studied is obtained based on the limiting thermal, mechanical and hydrodynamic criteria presented above and maximising the heliostat-receiver efficiency. Once the optimum receivers have been obtained, the nominal power of each PB and the global efficiency of the different SPTs can be obtained. The efficiencies of the different SPTs have been compared at the design point

and at different power loads to determine which SPT design is the most suitable considering the expected operational conditions of the SPT. Finally, the investment cost of the different SPTs has been estimated to evaluate the main economical and technical advantages and disadvantages of each of the analysed SPTs.

5.1. Receiver selection

The results of the receiver geometry analysis are discussed in the following paragraphs. Moreover, the possibility of using different materials has been studied. Because Inconel 625 is the cheapest material, it has been proposed when the operational conditions allow for it without reducing the field-receiver efficiency. When Inconel 625 cannot be used, alloy 800H is the alternative, and only for the most extreme operational conditions has Haynes 230 been employed (see Figure 4).

The minimum allowable thickness of the tubes was known following a previous calculation of the receiver; in that calculation, it was assumed that all the receivers had a tube thickness of 1.65 mm. After this first approximation, the optimal thickness was determined as the nominal thickness closer to the minimum allowable thickness.

Figure 5 shows the minimum allowable thicknesses for the different geometries of the reference receiver (Sub1) composed of Inconel 625 using an aiming factor k=2. As shown, the minimum allowable thickness generally increases with the tube diameter and the number of panels. However, for small tube diameters and high number of panels, the minimum allowable thickness is higher than that for larger diameters due to the high internal pressure of these tubes. The same pattern for the analysed receivers has been obtained

for different materials and aiming factors.

Figure 6 shows the effect of the aiming strategy ($k = 1.5$, $k = 2$ and $k = 2.5$), the number of panels and the tube diameter on the main operational parameters for the reference receiver: film temperature, combined field-receiver efficiency (see Equations 3 and 4), mechanical stress and pressure drop. Figure 6 presents these parameters for the optimum thickness obtained from Figure 5.

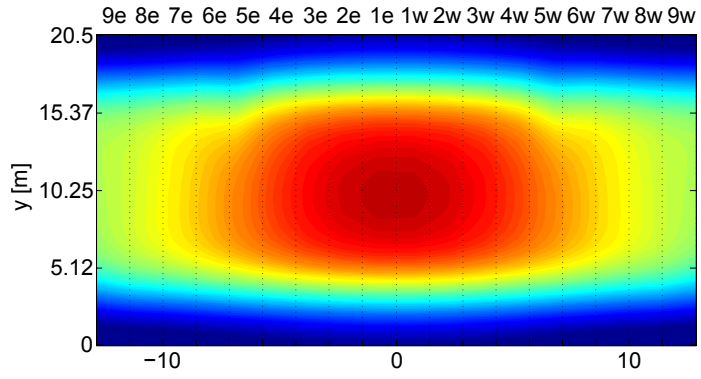

(a)

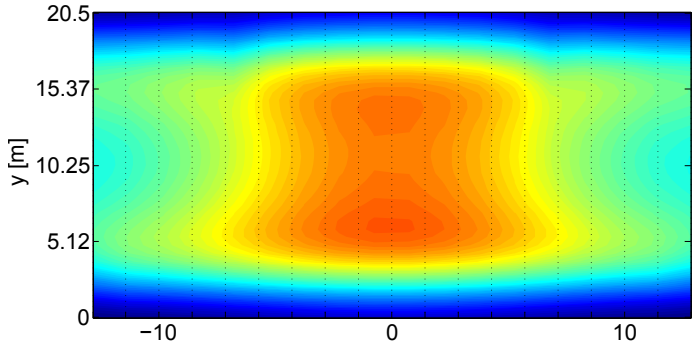

(b)

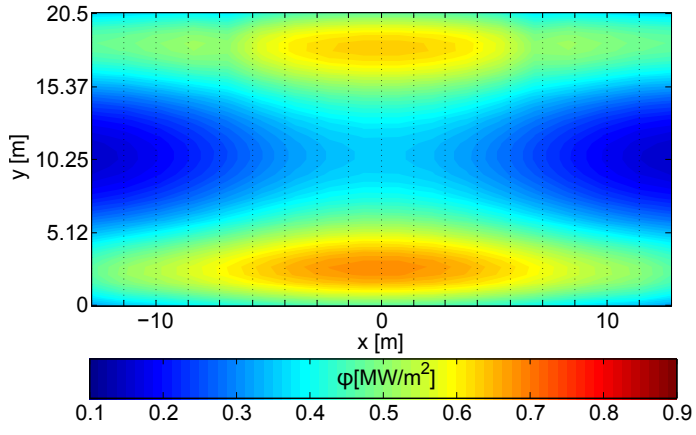

(c)

Figure 3: Solar flux density intercepted by a receiver formed by 18 panels at solar noon of the spring equinox. Each sub-figure corresponds to different aiming factors: a) k=2.5, b) k=2, and c) k=1.

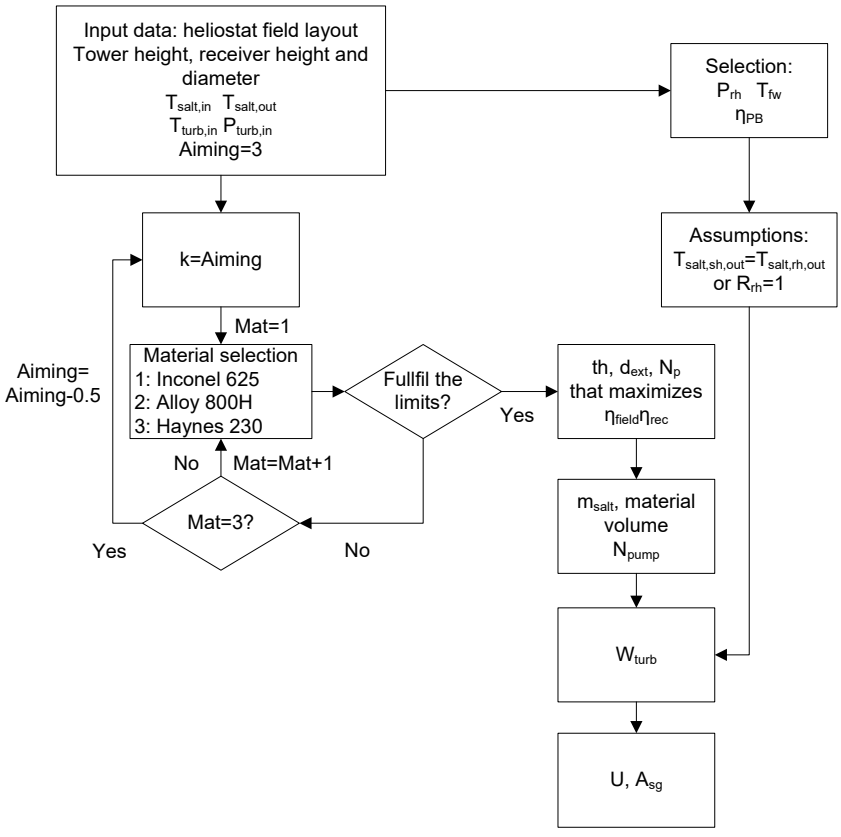

Figure 4: Flowchart for the SPT design.

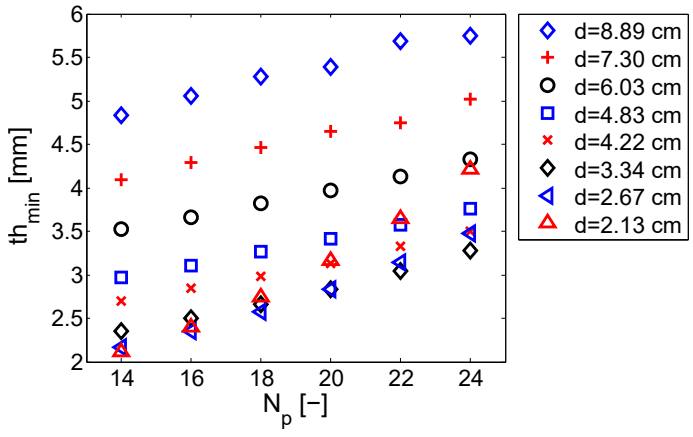

Figure 5: Minimum allowable tube thickness, th_{min}, for different geometries of the reference receiver (Sub1) composed of Inconel 625 and using k=2.

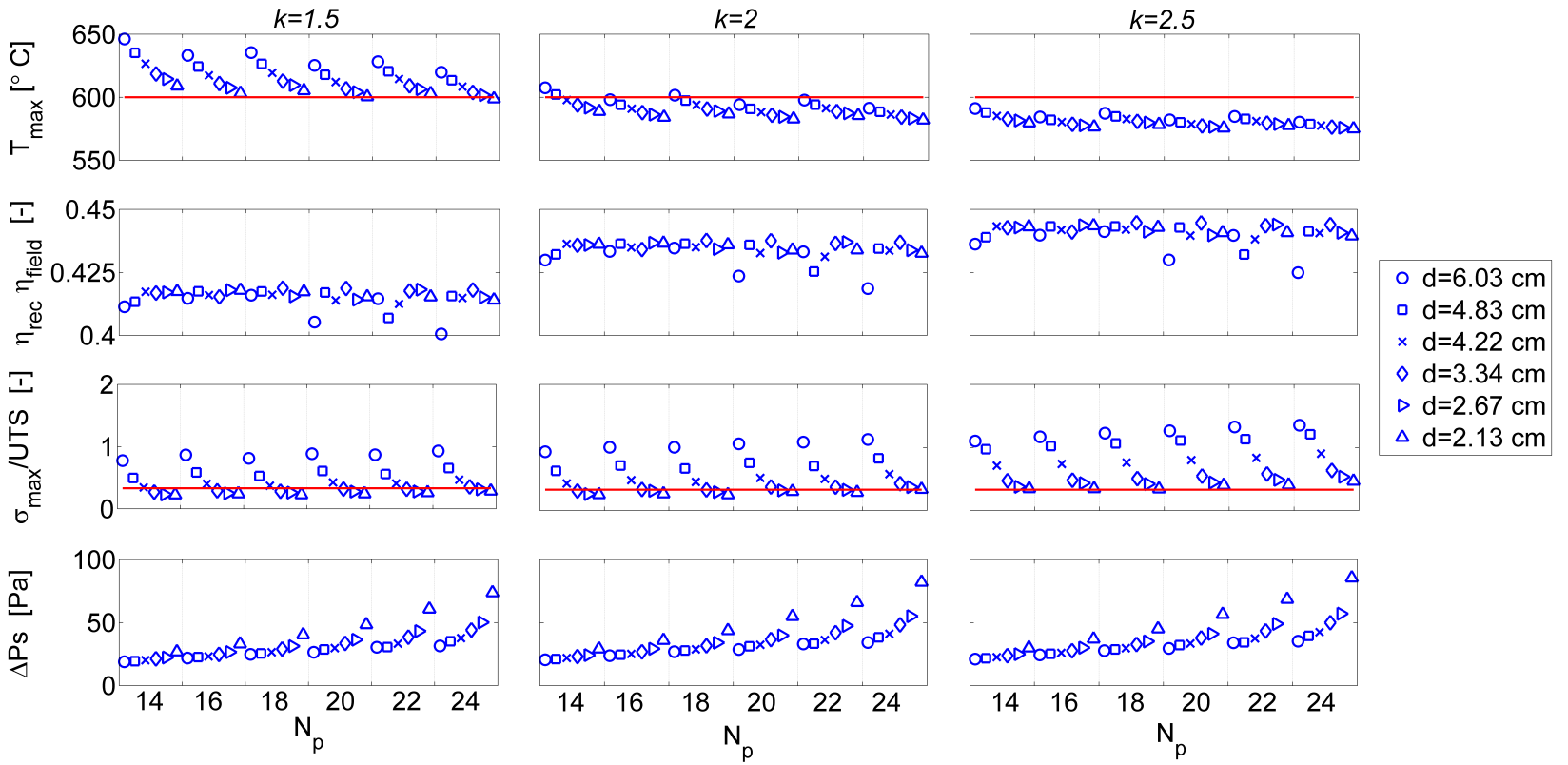

Figure 6: Effect of the aiming factor, the number of panels and the tube diameter on the film temperature ($T_{film,max}$), combined heliostat-receiver efficiency ($\eta_{rec}\eta_{field}$), mechanical stresses (σ_{max}) and pressure drop (ΔPs) for the reference receiver composed of Inconel 625.

The aiming strategy is a decisive factor in the growth of the mechanical stresses. With aiming factors of 2.5 or higher, the mechanical stresses exceed the material limit; thus, the use of aiming factors higher than 2 does not ensure safe operation of the receivers.

Nevertheless, the film temperature decreases when the aiming factors increase due to a change in the mass flow rate, which increases the global coefficient of heat transfer in the receiver. Then, the thermal efficiency of the receiver also increases as the aiming factor increases. For the reference receiver, shown in Figure 6, the average mass flow rate increases from 960 kg/s at $k = 1.5$ to 1020 kg/s at $k = 2.5$, representing an increase of 3.5% of the combined field-receiver efficiency. Therefore, the aiming factor should be as high as the mechanical limitations of the materials withstand, which in the reference receiver corresponds to $k = 2$.

Regarding the receiver geometry, Figure 6 shows that the film temperature decreases with the number of panels. A higher number of panels means narrower panels and a lower number of tubes per panel, increasing the salt velocity and the global heat transfer coefficient. Although a larger tube diameter reduces the number of tubes per panel, the salt velocity decreases due to an increase in the cross-sectional area. Then, higher tube diameters correspond to larger film temperatures.

Figure 6 also shows that the mechanical stress increases with the tube diameter and decreases with the number of panels. The mechanical stress presents problems for large tube diameters and $k > 2$.

The total pressure drop increases with the number of panels and decreases with the tube diameter.

The combined field-receiver efficiency is almost constant with the number of panels and the tube diameter. However, there are some geometries for which the efficiency decreases because it is a function of the effective surface of radiation. Hence, the efficiency is lower for non-compact receivers, i.e., the use of 20 or 24 panels with a tube diameter of 6.03 cm is not recommend for the selected receiver dimensions.

To select the optimum receiver, the factors explained above have been evaluated in the following order. First, only the mentioned optimum thickness for each receiver geometry was considered. Second, all the receiver designs in which the film temperature and the mechanical stresses exceeded the limit of the corresponding material were discarded. Once most of the receiver geometries were rejected, the optimum receiver was selected based on the maximum optical efficiency of the field (high k). In the case of several configurations with similar combined heliostat-receiver efficiency, the receiver with the lowest pressure drop was selected. Table 3 presents the main parameters of the selected receivers for the eight SPTs analysed.

As shown in Table 3, the receivers that work at 565 °C can be constructed using Inconel 625. However, for higher temperatures, the material has to be replaced by Alloy 800H or by Haynes 230 in the case of Sup4, which works at the highest range of temperatures. The optimal receiver for all the studied SPTs should have 14 panels, and the optimal tube diameter varies from 42.2 mm to 26.7 mm. The optimal tube thickness for receivers composed of Alloy 800H is the lowest, 2.11 mm, due to the good performance of this material under corrosion. The optimal tube thickness for receivers composed of Inconel 625 is 2.77 mm, except for Sup1, which works at higher pressure

Table 3: Main parameters of the different SPTs analysed.

	Sub1	**Sub2**	**Sub3/Sup3**	**Sub4/Sup4**	**Sup1**	**Sup2**
Material	625	800H	625	800H	625	230
$\mathbf{N}_p$ **[-]**	14	14	14	14	14	14
$\mathbf{d}_{ext}$ **[mm]**	42.2	26.7	42.2	26.7	33.4	33.4
$\mathbf{N}_t$ **[-]**	87	138	87	138	110	110
th [mm]	2.77	2.11	2.77	2.11	3.73	9.09
Weight [ton]	70.5	50.6	70.5	50.6	90.4	191.8
Price [$/kg]	25	60	25	60	25	80
k **[-]**	2	2	2	2	1.5	1.5
η_{field} **[%]**	55.23	55.23	55.23	55.23	53.1	53.1
η_{rec} **[%]**	78.91	79.12	78.88	79.08	78.3	78.22
$\dot{m}$ **[kg/s]**	1000	900	1065	950	1630	1395
ΔP **[MPa]**	2.4	2.73	2.75	3.01	7.4	5.5
N_{pump} **[-]**	3pr	3pr	4pr	3pr	5pr x 2sr	4pr x 2sr
$\mathbf{T}_{wall,max}$ **[°C]**	769	736	775	734	740	765
σ_{max} **[MPa]**	137	82	150	82	146	124

and requires a thickness of 3.73 mm. Finally, Sup2 composed of Haynes 230 would need a tube thickness of at least 9.09 mm; the utilisation of the latter thickness is infeasible for transient conditions, and thus, the SPT Sup2 cannot be employed in the current SPT.

In subcritical and supercritical SPTs with low reheating pressure, an aiming factor of 2 is the most suitable. However, in supercritical SPTs with high reheating pressure, the aiming factor has to be lower to fulfill the film

temperature limitation: it reduces the optical efficiency of the heliostat field.

The efficiency of the receivers is almost constant. Then, the combined field-receiver efficiency of the supercritical SPT with a high reheating pressure is the lowest; thus, the increase in the global efficiency of the SPTs is less than expected considering only the PB efficiency. To keep the combined efficiency in these plants constant, smaller heliostats would be required to reduce spillage losses, but at the expense of increasing the investment cost associated with the heliostat field. For the other six SPTs, the global efficiency of the SPTs mainly depends on the PB efficiency.

In Table 3, it is also observed that the mass flow rate in SPTs Sup1 and Sup2 significantly increases; hence, a higher number of feed pumps have to work in parallel. In these plants, the pressure drop also increases, thus further decreasing the global efficiency of the SPT and increasing the number of required feed pumps working in series.

Finally, Table 3 presents the maximum tube wall temperature and mechanical stresses reached by the receivers. As shown, lower mechanical stresses are found in the receivers composed of Alloy 800H because it has the worst mechanical properties and cannot withstand high stresses. In contrast, for the other two materials, the maximum allowable mechanical stresses are similar. In all cases, the maximum stresses are found in the first panel of the receivers.

The maximum tube wall temperature is similar for the different receivers analysed: it varies between 734 °C (Sub4/Sup4) and 775 °C (Sub3/Sup3). The wall temperature distribution is presented in Figure 7; note that the behaviour of each panel is displayed by a representative tube having a total of

14 representing tubes in each receiver. It can be observed that the maximum wall temperature is reached in the external surface of the southern panels. However, it is located in the middle of the tube for large aiming factors and in the edges of the tubes for low aiming factors (Sup1 and Sup2).

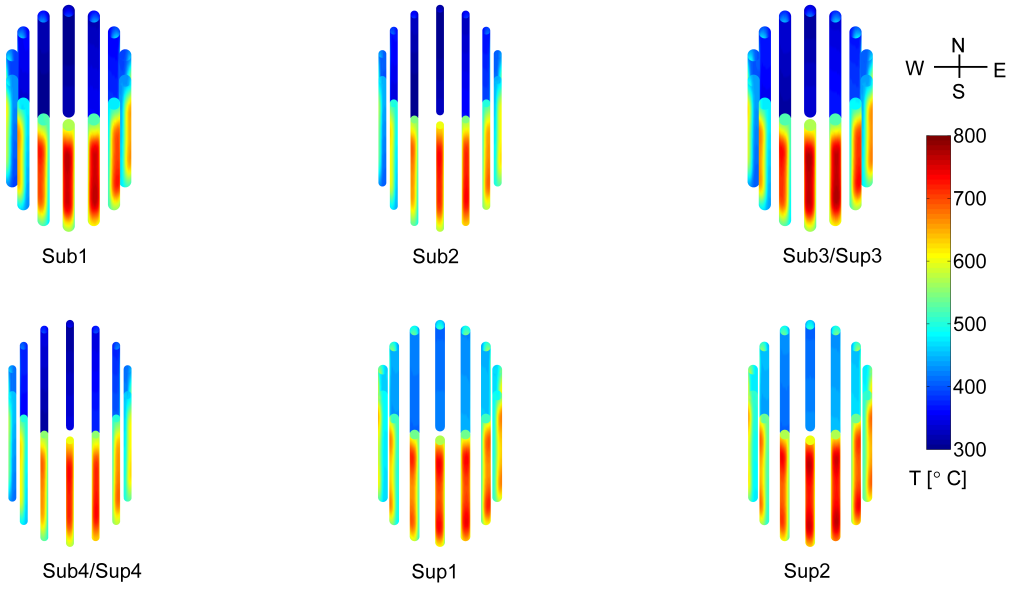

Figure 7: Wall temperature map of the six selected receivers (see Table 3) at nominal power.

5.2. Comparison of SPTs

The obtained efficiencies of the main subsystems of the eight analysed SPTs using the optimal receiver configurations are shown in Figure 8. The PB efficiency was obtained from the literature, as shown in Table 1. The receiver and heliostat field efficiencies were calculated using the model explained previously, and the SPT efficiency was calculated as the product of

the efficiencies of the three subsystems, as shown in Equation 1. Moreover, adding the parasitic consumption of the feed pump systems was performed to calculate the effective efficiency of the SPT.

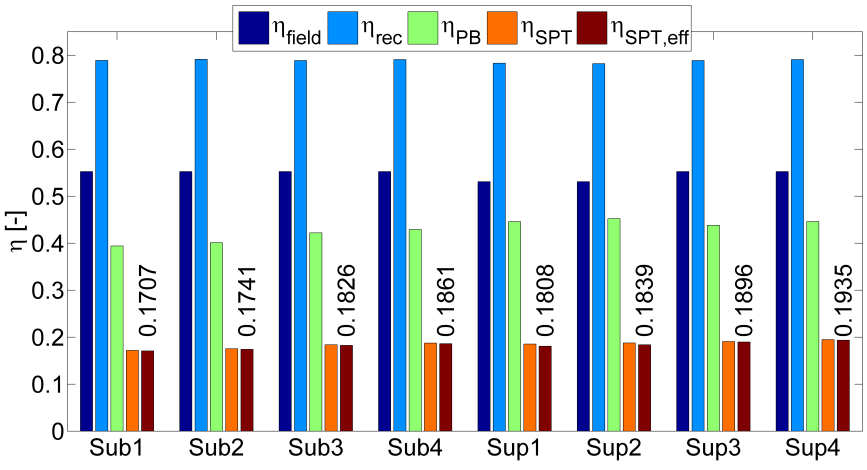

Figure 8: Efficiencies at nominal load for the main subsystems of the eight SPTs analysed.

As shown in Figure 8, the reference SPT is the one with the lowest global efficiency. At the same time, it is observed that both the temperature and the pressure of the steam increase the SPT efficiency, with the effect of the pressure being more important. In contrast, for high reheating pressure, the efficiency increases more slowly.

On the one hand, if the pressure at the inlet of the turbine is increased from 12 (Sub1) to 16 MPa (Sub3) while maintaining the temperature and the reheating pressure constant, the SPT efficiency increases 1.19% with respect to the reference SPT (Sub1). If the pressure is 24 MPa (Sup3), the efficiency increases 1.89%, and if the reheating pressure increases with an inlet pressure of 24 MPa (Sup1), the global efficiency only increases 1% with

respect to the reference case. On the other hand, if the temperature varies from 548 °C (Sub1) to 580 °C the SPT efficiency increases approximately 0.4%, regardless of the pressure.

Therefore, the best global efficiency is found in Sup4, whose efficiency improvement with respect to the reference SPT is 2.28%; note that it is less than one half of the improvement obtained by its PB, which represents a 5.2% improvement.

Other SPTs with high global efficiency are Sup3 and Sub4. Note that although the PB efficiency of Sup1 is 1.7% higher than for Sub4, the global SPT efficiency of the supercritical SPT is 0.5% lower than that for Sub4.

5.3. Off-design conditions

In this subsection, the average efficiency of the receiver operating off-design has been calculated. The model developed by Rodríguez-Sánchez et al. (2015a) to estimate the receiver efficiency at partial load has been employed.

The efficiency of the heliostat field is constant at different power loads because the aiming strategy has been assumed to be the same. However, the availability of the field and/or the solar resource decreases at partial power load. In molten salt SPTs, the PB typically works independently of the solar receivers thanks to the thermal storage. Thus, it has been assumed that the PB always works at nominal load (Kolb, 2011). Then, at partial load, only the receiver efficiency has been modified, as shown in Equation 8,

$$\frac{\eta'_{rec}}{\eta_{rec}} = \frac{(\phi'_{inc} - L'_{thl})\,\phi_{inc}}{(\phi_{inc} - L_{thl})\,\phi'_{inc}} \tag{8}$$

where L_{thl} are the thermal losses of the receiver at nominal power load, L'_{thl} represent the thermal losses at partial load, and ϕ'_{inc} and ϕ_{inc} correspond to the part and the nominal incident solar flux, respectively.

Figure 9(a) depicts the efficiency of the six receivers studied as a function of the incident power. It can be observed that the receiver efficiency decreases with the load. At nominal power load, the efficiency of all the receivers is similar, being slightly lower for Sup1 and Sup2. However, the reduction of the efficiency at small power loads is more pronounced in these receivers, particularly in Sup2, due to the decrease in the global coefficient of heat transfer.

Figure 9(b) presents the effective global efficiencies of the eight SPTs analysed for different incident powers, and it is observed that supercritical SPTs are the most efficient SPTs for high power loads; nevertheless, Sup2 becomes the least efficient SPT for power loads lower than 35%. Sup1 also becomes the second least efficient SPT for power loads under 20%. Although the remainder of the SPTs have similar efficiencies at nominal power, all of them equalise their efficiencies at 10% of the power load.

Therefore, the most recommended SPT is Sup4, followed by Sup3 and by subcritical SPTs. Sup1 and Sup2 could be recommended only for SPTs in which the expected operational conditions are always at high power load.

5.4. Cost analysis

To complete the SPT comparison, the relative investment cost of the different SPTs studied has been analysed. Figure 10 presents the investment costs of the different SPTs analysed. Because the heliostat field cost for the eight SPTs is the same, the cost is primarily a function of the PB, the receiver

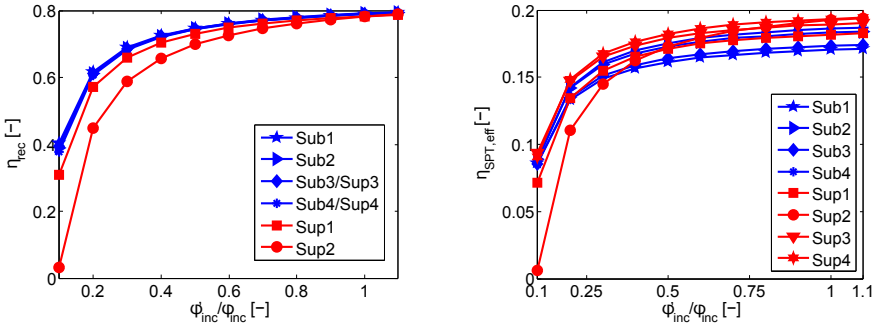

(a) (b)

Figure 9: a) Thermal efficiency of the eight receivers analysed as a function of the incident solar flux. b) Global effective efficiency of the eight SPTs analysed as a function of the incident solar flux in the receivers.

material and the number of feed pumps.

Kolb et al. (2007) estimated the price of the installed heliostats in 2006 as 126 \$/m^2 for a production of 50,000 heliostats per year; 7 years later, Bhargav et al. (2013) obtained comparable results. Because the production rate of the heliostats has not notably increased since then, the economies of scale have not yet affected the heliostats. Then, the investment cost for the heliostat field has been estimated to be 150.8 M\$.

The receiver cost is based on the properties (ASME, 2011) and on the price of each tube material, which are collected from tube suppliers (see Table 3). The price obtained for the subcritical receivers is in agreement with the prices given by Augsburger (2013), who claimed that the cost of molten salt receivers is approximately 127 \$/KW$_{thl}$. Moreover, in the price of the receiver has been included the price of the tower, of the piping circuit and of 6 hours of thermal energy storage (TES), which includes the price of the vertical pumps (Cheang et al., 2015; Pacheco et al., 2013; Singer et al.,

2014). The price of each feed pump used in this analysis is approximately 350,000 $.

The PB cost primarily depends on the pressure of the cycle, steam generator and heat exchanger. The heat exchanger price of subcritical and supercritical steam generators has been estimated using the model proposed by Purohit (1983). This method takes into account several parameters such as: heat transfer area, shell and tube material, shell and tube side pressure, tube thickness, etc. The supercritical steam generators have been considered as straight tube/straight shell heat exchangers in order to estimate the investment cost using the Purohit method.

The materials selected for the shells and tubes of the heat exchangers of the subcritical steam generators were stainless steel (Gr-347) for reheater and superheater, low chrome alloy steel (9Cr - 1Mo) for evaporator and carbon steel for preheater (Zavoico, 2001). The material selected for the shells and the tubes of the heat exchangers of the supercritical steam generators was stainless steel (Gr-347).

For subcritical turbines, the cost estimated by Kolb (2011) is approximately 800 \$/kW$_e$, and it is only 861 \$/kW$_e$ for supercritical turbines (Pacheco et al., 2013).

Figure 10 presents the approximate investment cost for each SPT analysed. The costs of the analysed subcritical plants are comprised between 466 and 487 M\$, whereas the price of the supercritical plants is around 503 M\$ and 530 M\$. Moreover, it can be observed that the price of the solar field and the power block are similar in the subcritical SPTs, but the cost of the PB increases in supercritical SPTs, being the highest one.

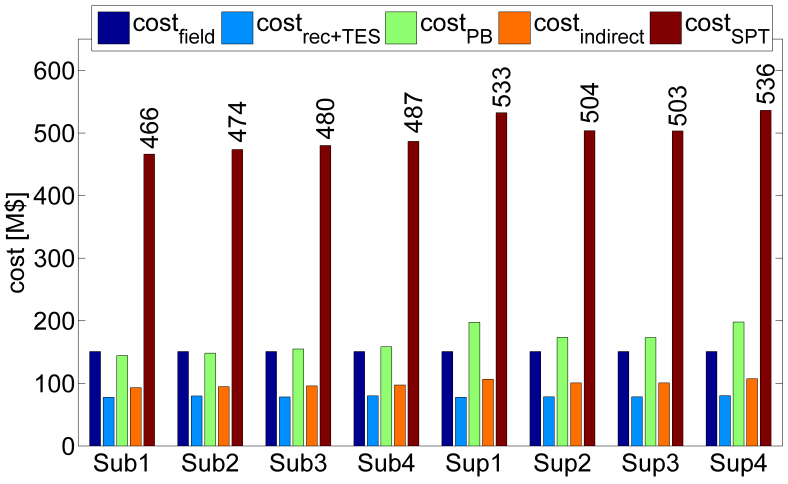

Figure 10: Cost analysis for the different subcritical and supercritical SPTs studied.

Table 4: Power and cost analysis for the different subcritical and supercritical SPTs studied.

	Sub1	**Sub2**	**Sub3**	**Sub4**	**Sup1**	**Sup2**	**Sup3**	**Sup4**
Thermal power [MW_{thl}]	418.33	419.41	418.16	419.20	399.00	398.56	418.16	419.20
Net nominal power [MW_e]	106.9	110.7	114.6	118.28	134.6	117.1	119.0	123.09
Cost per kW [$/$kW_e$]	4361	4279	4189	4115	3956	4301	4230	4358

Table 4 shows the net power generated by the different SPTs at nominal load. The net power is defined as the power generated by the SPT minus the parasitic consumption of the feed pump system. It can be observed that the SPTs working at 580 °C generated more power (approximately 4 MW_e) than its respective SPT working at 548 °C. Sup1 is the only exception because

the receiver of Sup1 works with the highest mass flow rate, around 250 kg/s extra.It suposse that Sup1 generates approximately 27 MW_e more than the reference SPT.

The net power generated by the subcritical SPTs working at 12 MPa is the lowest, generating 8 MW_e less than the other subcritical SPTs. The power generated by the subcritical SPTs working at 16 MPa is the same as that produced by Sup2 and slightly lower than that produced by the supercritical SPTs working at the same reheating pressure.

Sup2 is the SPT with highest cost per kW_e; thus, its use is discarded for mechanical and economical reasons. Sub1 and Sub2 are not recommended because although they have the lowest investment cost, the price per kW_e is not low enough. Although Sup1 has the highest investment cost, it generates the maximum electrical power due to the high efficiency of the steam-salt heat exchangers; thus, it has the lowest cost per kW_e. However, its use has to be discarded due to the poor performance at low power loads.

The next lowest cost per kW_e is Sub4. This SPT has a moderated investment cost. Moreover, it is the subcritical SPT that produces more electrical power, having a production close to the obtained with the more expensive supercritical SPTs with low reheating pressure. Therefore, subcritical SPTs designing with high pressure and temperature live steam seem to be the most promising technology with the prices taken in the analysis.

6. Conclusions

In this work, the feasibility of introducing a new generation of SPTs with higher temperatures and pressures has been analysed. Eight different sub-

critical and supercritical SPTs, whose conditions at the inlet of the turbine are a temperature of 548 °C or 580 °C and pressure of 12 MPa, 16 MPa or 24 MPa, have been studied. Moreover, the effect of the reheating pressure in the PB has been analysed, testing pressures of 4.5 MPa and 70 MPa.

The heliostat field for the eight SPTs is the same, while the receiver design, the PB and the feed pump system have been optimised for each of the SPTs studied. The PB efficiency of the new generation of SPTs is up to 5.8% higher than the current subcritical PB efficiency. However, the combined heliostat-receiver efficiency of these new SPTs is smaller. Subsequently, the reduction of the heliostat-receiver efficiency has been studied to determine which plant is more likely to remain in the near future.

The global efficiency of the SPT increases with the main steam temperature and pressure. In addition, special attention has to be paid to the reheating pressure. Contrary to the conventional supercritical power plants, the efficiency of the SPT decreases with high reheating pressure due to an important reduction in the combined heliostat-receiver efficiency. Thus, it is preferable to have a lower efficiency in the evaporator train than in the heliostat field or in the receiver. A way to increase the combined heliostat-receiver efficiency would be to install heliostats with a smaller size, but the cost of the SPT would increase considerably. Moreover, the minimum allowable tube thickness of these types of receivers has to be carefully studied because they cannot always provide transient conditions with safety.

For nominal conditions, the best SPT efficiency is approximately 19% for supercritical SPTs with a low reheating pressure, which represents a 2% better efficiency than Sub1. However, the effciency improvement obtained

compared to the reference plant is lower than the improvement of the PB efficiency. Subcritical SPTs working at 16 MPa cannot be forgotten because their global efficiency is only 0.3% lower than that for the supercritical plants working at the same reheating pressure.

The efficiency of the SPT decreases at low power loads; however, this decrease is highlighted in SPTs with high reheating pressures. If the reheating pressure is almost constant, the highest efficiency is found in SPTs with the highest steam pressure and temperature, although the parasitic consumption of the feed pump system generally reduces the differences.

The last factor considered in this study is the investment cost of the different SPTs. It has been shown that the investment cost of subcritical SPTs working at 12 MPa is the lowest, but they also have the lowest nominal power. Thus, SPTs working at higher pressure have to be implemented to reduce the cost per kW_e. From the analysed SPTs, the most recommendable, based on a thermo-economic analysis, is the implantation of subcritical SPTs working at high pressure and temperature, due to it has high efficiency and the lowest cost per KW_e. Thus, the best option is not to select the most efficient PB, else if it is required to reach a compromise between the combined heliostat-receiver efficiency, the PB efficiency and the investment cost of the SPT.

Nomenclature

A	Surface area [m^2]
d	Tube diameter [m]
H	Head of the pump [m]

k	Aiming strategy factor [-]
L	Heat losses [W]
$\dot{m}$	Mass flow rate [kg/s]
N	Number of elements [-]
p	Panel [-]
Ps	Pressure [Pa]
$\dot{Q}$	Volumetric flow rate [m^3/s]
S	Maximum allowable stress [Pa]
T	Temperature [°C]
t	Tube [-]
th	Thickness [m]
U	Global heat transfer coefficient [W/(m^2K)]
UTS	Ultimate tensile strength [Pa]
W	Work [W]
x	Perimetral coordinate [m]
y	Receiver height coordinate [m]

Greek symbols

α	Absorptivity [-]
β	Incident angle (cosine factor) [-]
ΔP	Pressure drop [Pa]
η	Efficiency [-]
ϕ	Solar flux density [W/m^2]
ρ	Reflectivity [-]

σ	Mechanical stress [Pa]

606 *Subscripts*

abs	Absorbed
at	Atmospheric
corr	Corrosion
eff	Effective
ext	External
fw	Feed water
h	Heliostat
in	Inlet
inc	Incident
int	Internal
out	Outlet
ps	Pressure
p	Panel
rec	Receiver
sg	steam generator
sh	superheater
sp	Spillage
s&b	Shade and block
rh	reheater
t	Tube
thl	Thermal
turb	Turbine

Abbreviations

Amb	Ambient
HP	High pressure
HTF	Heat transfer fluid
LCOE	Levelized cost of electricity
LP	Low pressure
PB	Power block
pr	Parallel
RW	Refractory wall
SPT	Solar power tower
sr	Serial
Sub1	Subcritical plant at 12 MPa and 548 °C
Sub2	Subcritical plant at 12 MPa and 580 °C
Sub3	Subcritical plant at 16 MPa and 548 °C
Sub4	Subcritical plant at 16 MPa and 580 °C
Sup1	Supercritical plant at 24 MPa and 548 °C
Sup2	Supercritical plant at 24 MPa and 580 °C
TES	Thermal energy storage

Acknowledgements

This work has been supported by the Spanish government under the projects ENE2012-34255 and ENE2015-69486-R. Moreover, the authors would like to thank Friatec for the curves and data provided for the molten salt pump.

References

Alexe, F., Cenusa, V., 2008. Comparaatively optimizing the feed water pre-heat and the reheat pressure for condensing steam cycles. Electrotehnica, energetica, electronica 3, 503–510.

Aliaxis, 2016. GVSO pump.
URL https://rheinhuette.de/pumpen/gvso-vertikale-chemie-kreiselpumpe-aus-metal

ASME, 2011. Boiler and Pressure Vessel Code, Section II - Materials. Tech. rep., American Society of Mechanical Engineers, New York.

Augsburger, G., 2013. Thermo-economic optimisation of large solar tower power plants. Ph.D. thesis, École Polytechnique Fédérale de Lausanne.

Bechtel corporation, 1993. Investigation of Thermal Sotorage and Steam Generor Issues. Tech. rep., Sandia National Laboratories, San Francisco, SAND93-7084.
URL http://www.osti.gov/scitech/servlets/purl/10189397

Bhargav, K. R., Gross, F., Schramek, P., 2013. Life cycle cost optimized heliostat size for power towers. Energy Procedia 49, 40–49.
URL http://dx.doi.org/10.1016/j.egypro.2014.03.005

Bloch, H. P., Singh, M. P., 2009. Steam Turbines Design, Applications, and Rerating, 2nd Edition. New York.

Boerema, N., Morrison, G., Taylor, R., Rosengarten, G., Sep. 2012. Liquid sodium versus Hitec as a heat transfer fluid in solar thermal central

receiver systems. Solar Energy 86 (9), 2293–2305.
URL http://www.sciencedirect.com/science/article/pii/S0038092X12001703

Boerema, N., Morrison, G., Taylor, R., Rosengarten, G., Nov. 2013. High temperature solar thermal central-receiver billboard design. Solar Energy 97, 356–368.
URL http://linkinghub.elsevier.com/retrieve/pii/S0038092X1300368X

Bradshaw, R. W., 1987. Thermal Convection Loop Study of the Corrosion of Incoloy 800 in Molten NaNO3-KNO3. Corrosion-Nace 43 (3), 173–178.

Cheang, V., Hedderwick, R., McGregor, C., 2015. Benchmarking supercritical carbon dioxide cycles against steam Rankine cycles for Concentrated Solar Power. Solar Energy 113, 199–211.
URL http://dx.doi.org/10.1016/j.solener.2014.12.016

Kolb, G., Jones, S., Donnelly, M., Gorman, D., Thomas, R., Davenport, R., Lumia, R., 2007. Heliostat Cost Reduction Study. Tech. Rep. June, SANDIA National Laboratories, Albuquerque, SAND2007-3293.

Kolb, G. J., 2011. An Evaluation of Possible Next-Generation High-Temperature Molten-Salt Power Towers. Tech. Rep. December, Sandia National Laboratories, Alburquerque and Livermore, SAND20011-9320.

Lovegrove, K., Stein, W., 2012. Concentrating solar power technology: principles, developments and applications. Woodhead publishing, Cambridge (U.K.).

McConohy, G., Kruizenga, A., May 2014. Molten nitrate salts at 600 and 680 C: Thermophysical property changes and corrosion of high-temperature

nickel alloys. Solar Energy 103, 242–252.
URL http://linkinghub.elsevier.com/retrieve/pii/S0038092X14000462

McGovern, R. K., Smith, W. J., Aug. 2012. Optimal concentration and temperatures of solar thermal power plants. Energy Conversion and Management 60, 226–232.
URL http://www.sciencedirect.com/science/article/pii/S019689041200074X

Modest, F. M., 2003. Radiative Heat Transfer. In: Radiative Heat Transfer, second edi Edition. Elsevier Science, New York, San Francisco, London, Ch. 5. RADIATI, pp. 162–197.

Neises, T. W., Wagner, M. J., Gray, A. K., 2014. Structural Design Considerations for Tubular Power Tower Receivers Operating at 650 C. Tech. Rep. April, NREL.

NREL, 2011. NREL: National Renewable Energy Laboratory.
URL http://www.nrel.gov/csp/solarpaces/by_project.cfm

Olivares, R. I., Sep. 2012. The thermal stability of molten nitrite/nitrates salt for solar thermal energy storage in different atmospheres. Solar Energy 86 (9), 2576–2583.
URL http://linkinghub.elsevier.com/retrieve/pii/S0038092X12002034

Pacheco, J. E., Wolf, T., Muley, N., 2013. Incorporating Supercritical Steam Turbines into Advanced Molten-Salt Power Tower Plants : Feasibility and Performance. Tech. Rep. March, Sandia National Laboratories, Albuquerque, SAND2013-1960.
URL http://prod.sandia.gov/techlib/access-control.cgi/2013/131960.pdf

Peterseim, J., Veeraragavan, a., 2015. Solar Towers with Supercritical Steam Parameters - is the Efficiency Gain worth the Effort? Energy Procedia 69 (0), 1123–1132.
URL http://linkinghub.elsevier.com/retrieve/pii/S1876610215004877

Petukhov, B., 1970. Heat Transfer and Friction in Turbulent Pipe Flow with Variable Physical Properties. Vol. 6. Moscow (USSR).

Purohit, G., 1983. Estimating costs of shell and tube heat exchangers. Chemical Engineering August, 22, 56–67.

Retzlaff, K., Ruegger, W., 1996. Steam turbines for ultrasupercritical power plants. Tech. rep., General Electric, Schenectady, NY, GER-3945A.

Rodríguez-Sánchez, M. R., Sánchez-González, A., Marugáan-Cruz, C., Santana, D., 2015b. Flow patterns of external solar receivers. Solar Energy 122, 940–953.

Rodríguez-Sánchez, M. R., Sánchez-González, A., Marugán-Cruz, C., Santana, D., 2014c. New Designs of Molten-salt Tubular-receiver for Solar Power Tower. Energy Procedia 49, 504–513.
URL http://www.sciencedirect.com/science/article/pii/S1876610214005086

Rodríguez-Sánchez, M. R., Sánchez-González, A., Marugán-Cruz, C., Santana, D., Nov. 2014d. Saving assessment using the PERS in solar power towers. Energy Conversion and Management 87, 810–819.
URL http://www.sciencedirect.com/science/article/pii/S0196890414007158

Rodríguez-Sánchez, M. R., Sánchez-González, A., Santana, D., Dec. 2015a. Revised receiver efficiency of molten-salt power towers. Renewable and

Sustainable Energy Reviews 52, 1331–1339.
URL http://www.sciencedirect.com/science/article/pii/S1364032115008461

Rodríguez-Sánchez, M. R., Soria-Verdugo, A., Almendros-Ibáñez, J. A., Acosta-Iborra, A., Santana, D., Feb. 2014a. Thermal design guidelines of solar power towers. Applied Thermal Engineering 63 (1), 428–438.
URL http://www.sciencedirect.com/science/article/pii/S1359431113008028

Sánchez, M., Romero, M., Jul. 2006. Methodology for generation of heliostat field layout in central receiver systems based on yearly normalized energy surfaces. Solar Energy 80 (7), 861–874.
URL http://linkinghub.elsevier.com/retrieve/pii/S0038092X05002124

Sánchez-González, A., Santana, D., Feb. 2015. Solar flux distribution on central receivers: A projection method from analytic function. Renewable Energy 74, 576–587.

Sano, T., 2009. Development of the Ultra High Efficiency Thermal Power Generation Facility. In: India Energy Congress. pp. 1–11.

Short, W., Packey, D. J., 1995. A Manual for the Economic Evaluation of Energy Efficiency and Renewable Energy Technologies. Tech. Rep. March.

Singer, C., Giuliano, S., Buck, R., 2014. Assessment of Improved Molten Salt Solar Tower Plants. Energy Procedia 49, 1553–1562.
URL http://linkinghub.elsevier.com/retrieve/pii/S1876610214006183

Winter, C. J., Sizmann, R. L., L, V.-H. L., 1991. Solar Power Plants. Springer Berlin Heidelberg, Berlin, Heidelberg.
URL http://www.springerlink.com/index/10.1007/978-3-642-61245-9

Zavoico, A. B., 2001. Solar Power Tower: Design Basis Document. Tech. Rep. July, Sandia National Laboratory, San Francisco, SAND2001-2100.

Zhang, D., Narula, R., Koza, D., Wen, H., Miller, B., 2013. Ultra-supercritical coal power plants. Materials, technologies and optimisation . Woodhead Publishing, Oxfors, Cambridge, Philadelphia, New Delhi.